JOURNAL OF MATERIALS SCIENCE 25 (1990) 3053–3060

Fatigue of Al–Li alloys: mechanical properties, microstructure (TEM and SEM) and strain localization

Y. BRÉCHET, F. LOUCHET
Laboratoire Thermodynamique et Physico-Chimie Métallurgiques, E.N.S.E.E.G., I.N.P. Grenoble, BP. 75, 38402 Saint Martin d-Hères, France

T. MAGNIN
Ecole des Mines de St. Etienne, 158 Cours Fauriel, 42023 St Etienne Cedex, France

The fatigue behaviour of two binary Al–Li alloys (A, solid solution; B, containing δ' precipitates) is studied by macroscopic fatigue tests, and microscopic (SEM and STEM) observations. Two types of strain localization are found, appearing as two types of slip band in SEM, and as two types of substructure in TEM. These characteristics are ascribed to strain localization processes governed by strain amplitude for the former and strain rate for the latter.

1. Introduction

Because of their high modulus and low density, Al–Li alloys are of great interest in the aircraft industry. However, their low ductility and poor fatigue resistance remains a problem for their future use. In the case of alloys with a shearable precipitation, this low ductility has been attributed to planar slip [1, 2] and strain localization. The purpose of this paper is to investigate the most simple of the Al–Li alloys, the binary alloy, either as a solid solution (Al–0.7 wt % Li) or with shearable precipitates (Al–2.5 wt % Li). The mechanical properties in fatigue are characterized by stress–cumulative strain curves and cyclic hardening curves. The macroscopic aspects of strain localization are shown by scanning electron microscopy (SEM) observation and the underlying substructures (dislocations and precipitates) are investigated by transmission electron microscopy (TEM).

2. Materials and experimental procedure

Two alloys have been extensively studied: Al–0.7 wt % Li alloy which is a solid solution, and Al–2.5 wt % Li alloy aged at room temperature and presenting a fine homogeneous distribution of δ' phase (average radius of precipitates 1 nm).

Cylindrical fatigue specimens (15 mm gauge length, 6 mm diameter) were machined from bars. Symmetrical tension compression tests were carried out on the electropolished specimens (0.5 mm grain size) under

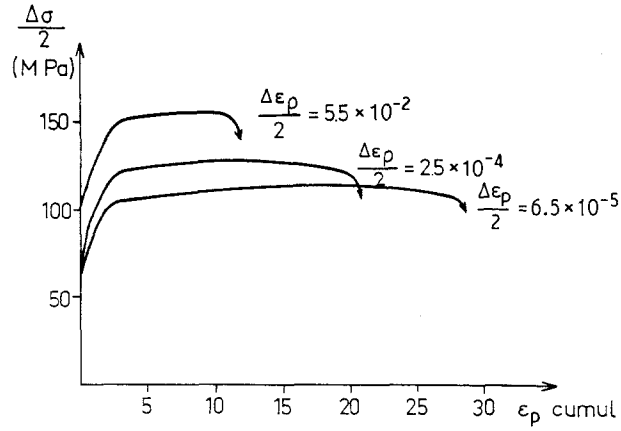

Figure 2 Cyclic hardening curves of the underaged Al–2.5% Li alloy.

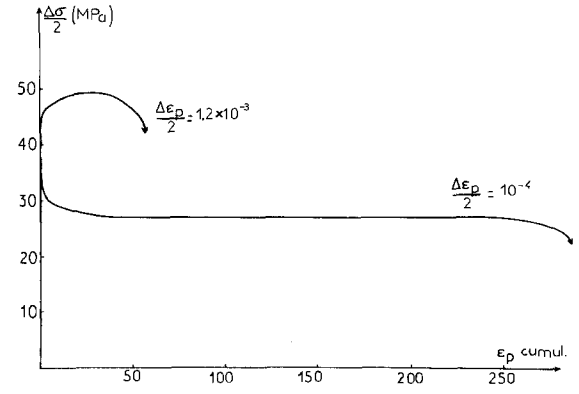

Figure 1 Cyclic hardening–softening curves of the Al–0.7% Li alloy ($\varepsilon_{p,cumul} = 4\Delta\varepsilon_p/2N$, N = number of cycles).

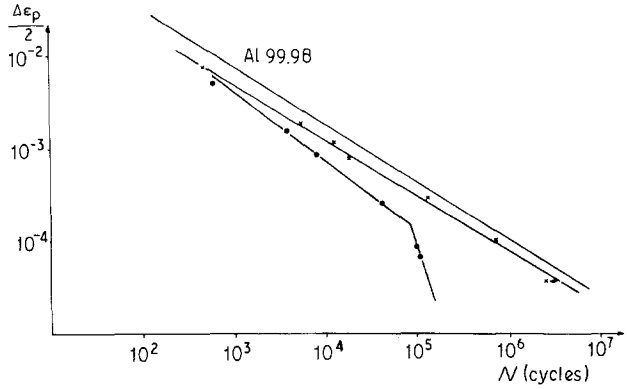

Figure 3 Coffin–Manson curves of the (x) Al–0.7% Li and (●) underaged Al–2.5% Li alloys.

0022–2461/90 $03.00 + .12 © *1990 Chapman and Hall Ltd.*

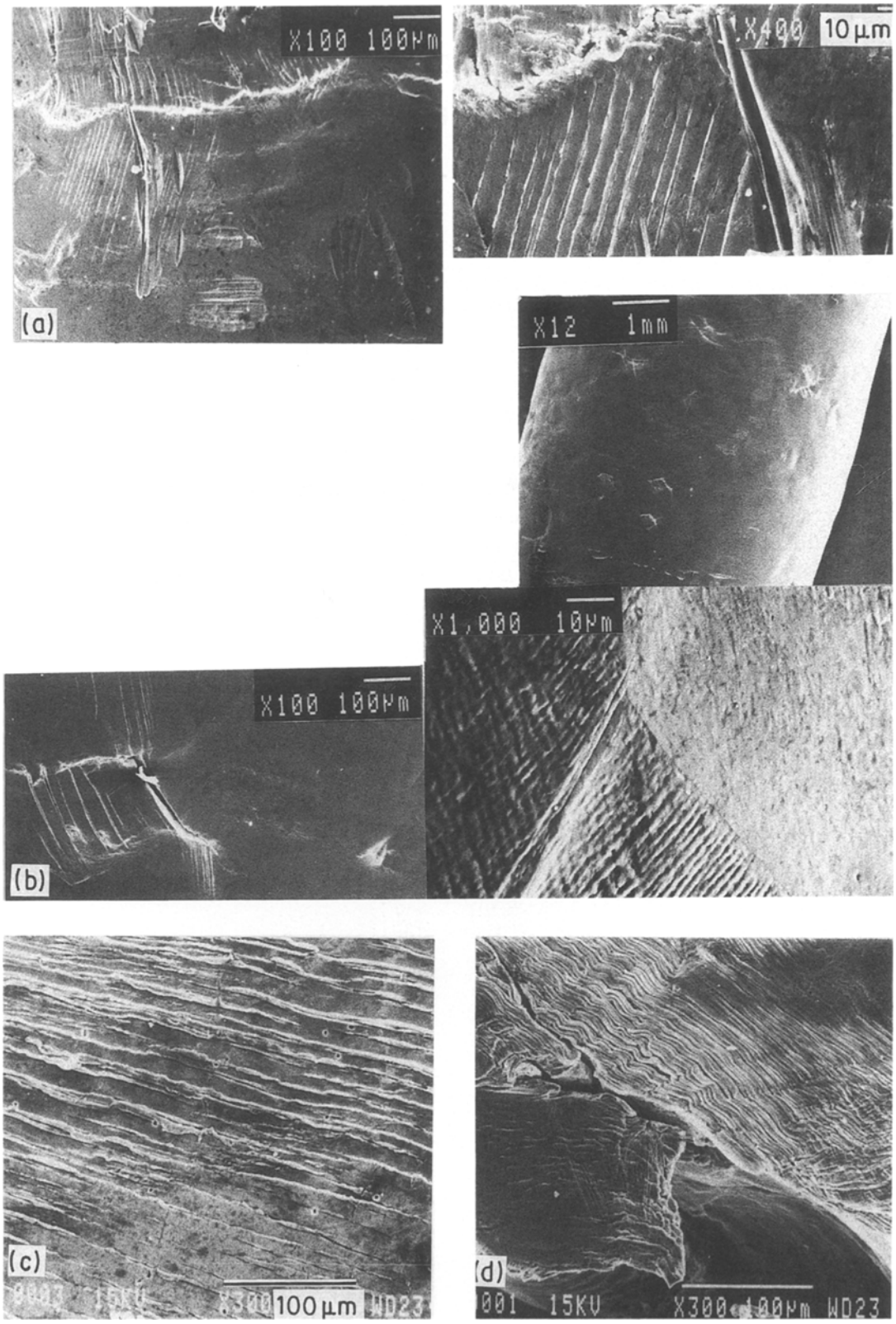

Figure 4 Al–0.7% Li alloy (SEM observation): (a) $\Delta\varepsilon_p/2 = 3 \times 10^{-4}$; (b) $\Delta\varepsilon_p/2 = 8 \times 10^{-4}$; (c) $\Delta\varepsilon_p/2 = 10^{-3}$; (d) $\Delta\varepsilon_p/2 = 1.5 \times 10^{-3}$.

constant plastic strain ($\Delta\varepsilon_p/2$) control, using a servo-hydraulic machine. Axial strain was measured by LVDT transducers. Fatigue tests were performed in the plastic strain range $5 \times 10^{-5} < \Delta\varepsilon_p/2 < 10^{-2}$ and a frequency $0.3 < f < 1$ Hz [3].

Thin foils were cut from each sample with a diamond saw. After reduction by mechanical thinning down to 0.3 mm, they were electropolished in a bath 1/3 HNO_3, 2/3 CH_3OH at $-15°$ C under 15 V. Observation of microstructures was done in a transmission electron microscope Jeol 200 CX. The localization of plastic deformation was investigated by surface observations with a JSM 840 scanning electron microscope.

3. Results

3.1. Mechanical testing

Figs 1 and 2 show the typical hardening–softening curves of the Al–0.7% Li alloy (Fig. 1) and the under-aged Al–2.5% Li alloy (Fig. 2). The following points can be noticed.

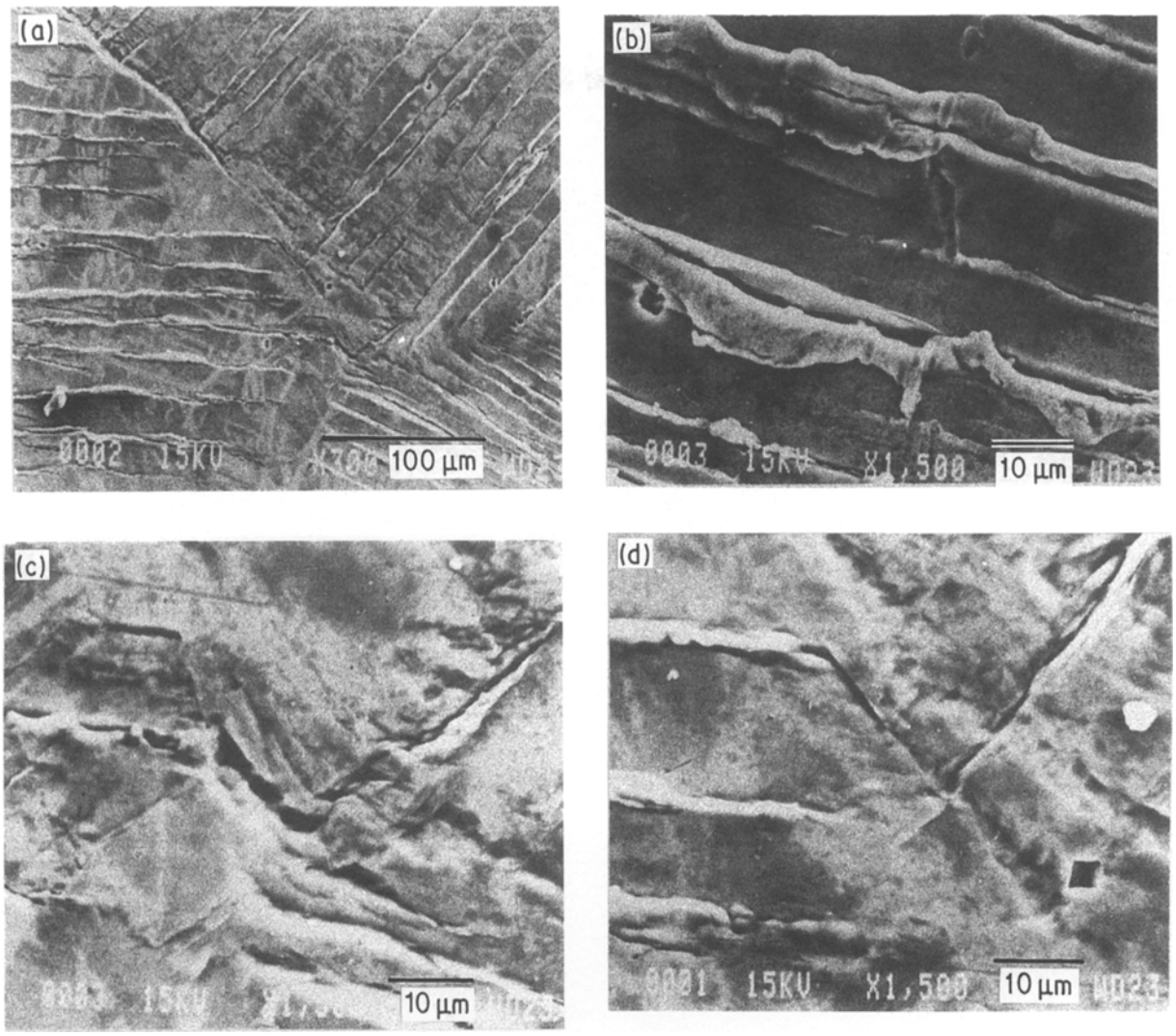

Figure 5 Al–0.7% Li alloy (SEM observation), $\Delta\varepsilon_p/2 = 10^{-3}$: (a) strain localization; (b) extrusions and intrusions observed at high magnification; (c) decohesion at triple point; (d) crack initiation at the intersection of a grain boundary and a slip band.

(i) For the Al–0.7% Li alloy, a rapid initial hardening is followed by slight softening and saturation at $\Delta\varepsilon_p/2 < 10^{-3}$. However, hardening is permanent at $\Delta\varepsilon_p/2 > 10^{-3}$ and no saturation occurs before a decrease of the maximum stress $\Delta\sigma/2$ due to crack nucleation.

(ii) For the underaged Al–2.5% Li alloy, all specimens exhibit rapid initial hardening followed by slow but persistent hardening up to crack initiation and failure. The Coffin–Manson curves ($\Delta\varepsilon_p/2$ plotted against the number of cycles to failure, N_f) are given by Fig. 3 for the different alloys.

It can be shown that: (a) the plot of the Al–0.7% Li alloy is quite parallel and close to that of pure aluminium [3]; (b) a change in slope seems to occur for the underaged Al–2.5% Li at low plastic strain amplitudes ($\Delta\varepsilon_p/2 < 2 \times 10^{-4}$). Moreover, this alloy exhibits a loss of fatigue resistance compared to the solid solution, particularly at low plastic strains.

3.2. SEM

SEM observations give evidence of strain localization. The behaviour is quite different in the solid solution and in the alloy with precipitates.

(i) For the solid solution, the inhomogeneity of deformation depends on the plastic amplitude imposed during fatigue:

for $\Delta\varepsilon_p/2 \leqslant 8 \times 10^{-4}$, deformation is almost homogeneous except in some places near the cracks (Figs. 4a, b);

for $\Delta\varepsilon_p/2 = 10^{-3}$ deformation is highly concentrated in narrow bands (Fig. 4c) the spacing of which is about 10 μm. The damaging influence of strain localization can be seen in this case (Figs 5a to d): large extrusions of metal can be seen, similar to those studied in copper [4]. When these slip bands arrive on a grain boundary (Fig. 5d), they create sites for cracks which propagate either along the slip band itself or along the grain boundary:

for $\Delta\varepsilon_p/2 = 7.5 \times 10^{-3}$ the deformation bands are much larger and their spacing is smaller: deformation again tends to become homogeneous (Fig. 4d).

(ii) For the alloy with shearable precipitates, two types of localization can be seen:

for $\Delta\varepsilon_p/2 \leqslant 3 \times 10^{-4}$ the localization of plastic deformation appears as very narrow and sharp slip lines but their spacing (about 1 μm) does not change with the applied strain amplitude. The larger the strain amplitude the coarser are the slip bands, but their spacing remains almost constant (Fig. 6a, b):

for $8.5 \times 10^{-4} \leqslant \Delta\varepsilon_p/2 < 2 \times 10^{-3}$ a second type of localization appears (Fig. 6c) the spacing

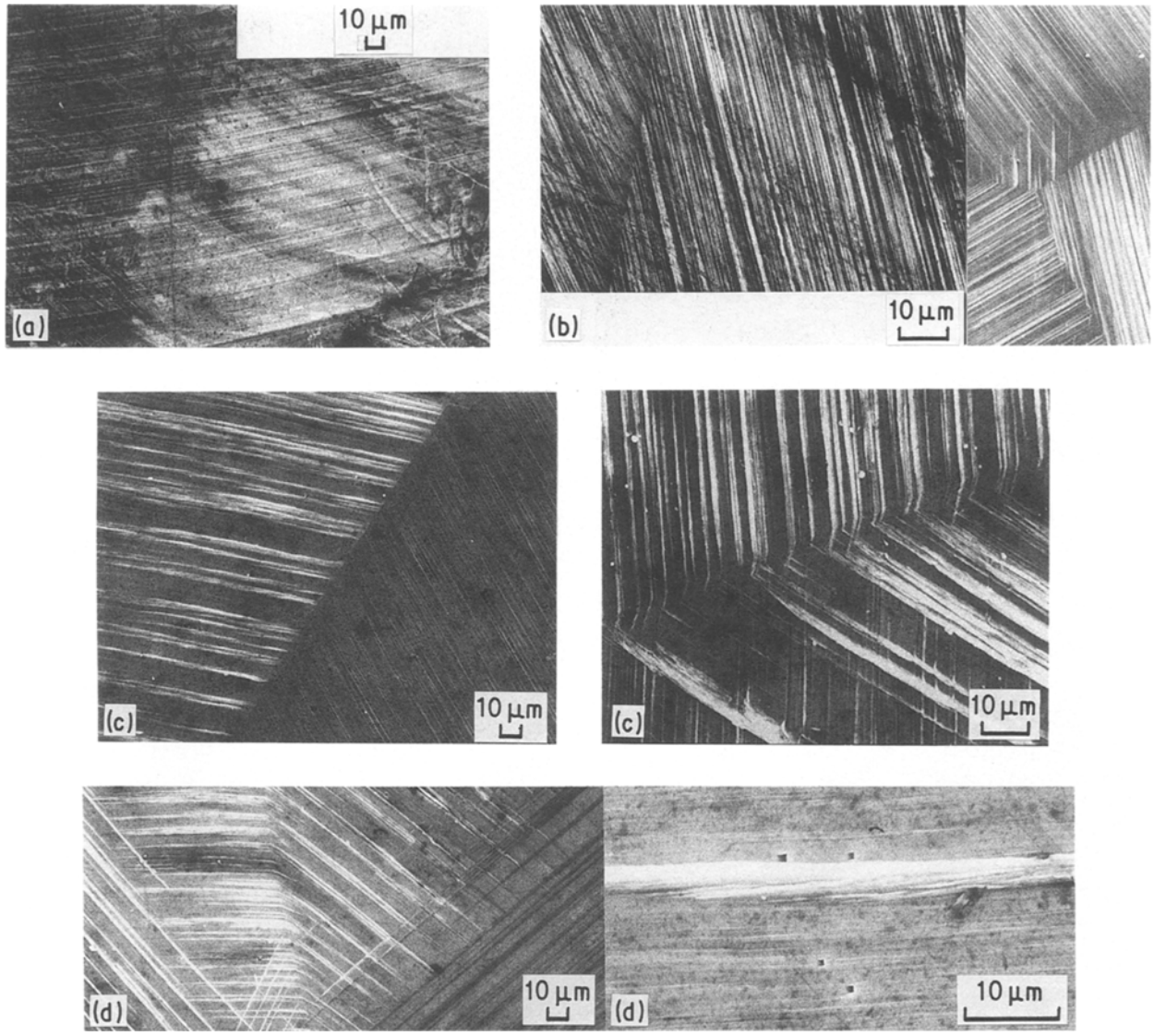

Figure 6 Al–2.5% Li alloy aged at room temperature (SEM observation). (a) $\Delta\varepsilon_p/2 = 5.5 \times 10^{-5}$. (b) $\Delta\varepsilon_p/2 = 3 \times 10^{-4}$, sharp lines, initiation of another system at a triple point. (c) $\Delta\varepsilon_p/2 = 8.5 \times 10^{-4}$. (d) $\Delta\varepsilon_p/2 = 2 \times 10^{-3}$; top right, detail of bands observed in top left; bottom, intergranular decohesion.

between these new bands which show marked extrusions, is about 10 μm: they seem to be the equivalent, for the alloy with δ' precipitates, of the localization bands observed in the solid solution (Fig. 6c).

for $\Delta\varepsilon_p/2 \geqslant 2 \times 10^{-3}$ the localization of the second type has disappeared and the morphology is again made of slip lines (Fig. 6d).

3.3. TEM

The strain localization is the macroscopic aspect of an inhomogeneity of dislocation structures or precipitation inside the material.

For the solid solution, when $1/2\Delta\varepsilon_p < 3 \times 10^{-4}$, that is when deformation is homogeneous, the unique dislocation substructure observed was made of cells (Figs 7a, b).

(i) When $1/2\Delta\varepsilon_p = 8 \times 10^{-4}$ the dominant structure is still a cellular one but sometimes a "channel" structure appears (Fig. 7c). The average size of cells (about 1.2 μm) does not evolve with $\Delta\varepsilon_p$ but the walls are better defined when $\Delta\varepsilon_p$ is larger.

(ii) When $1/2\Delta\varepsilon_p = 10^{-3}$, i.e. when deformation is highly localized, two structures are seen: on one side a cell structure identical to those we have observed at lower amplitude but with better defined walls, on the other side a labyrinth structure similar to that extensively studied in copper (Fig. 7d) [5]. The labyrinth structure is simply the equivalent with several Burgers vectors of the PSB structure observed in the case of single slip. Therefore, when deformation is localized, there is a highly deformable dislocation structure (labyrinth) which probably corresponds to the slip bands, and a less deformable structure (cells) which correspond to the less deformable parts of the material.

(iii) When $1/2\Delta\varepsilon_p = 7.5 \times 10^{-3}$ the deformation is

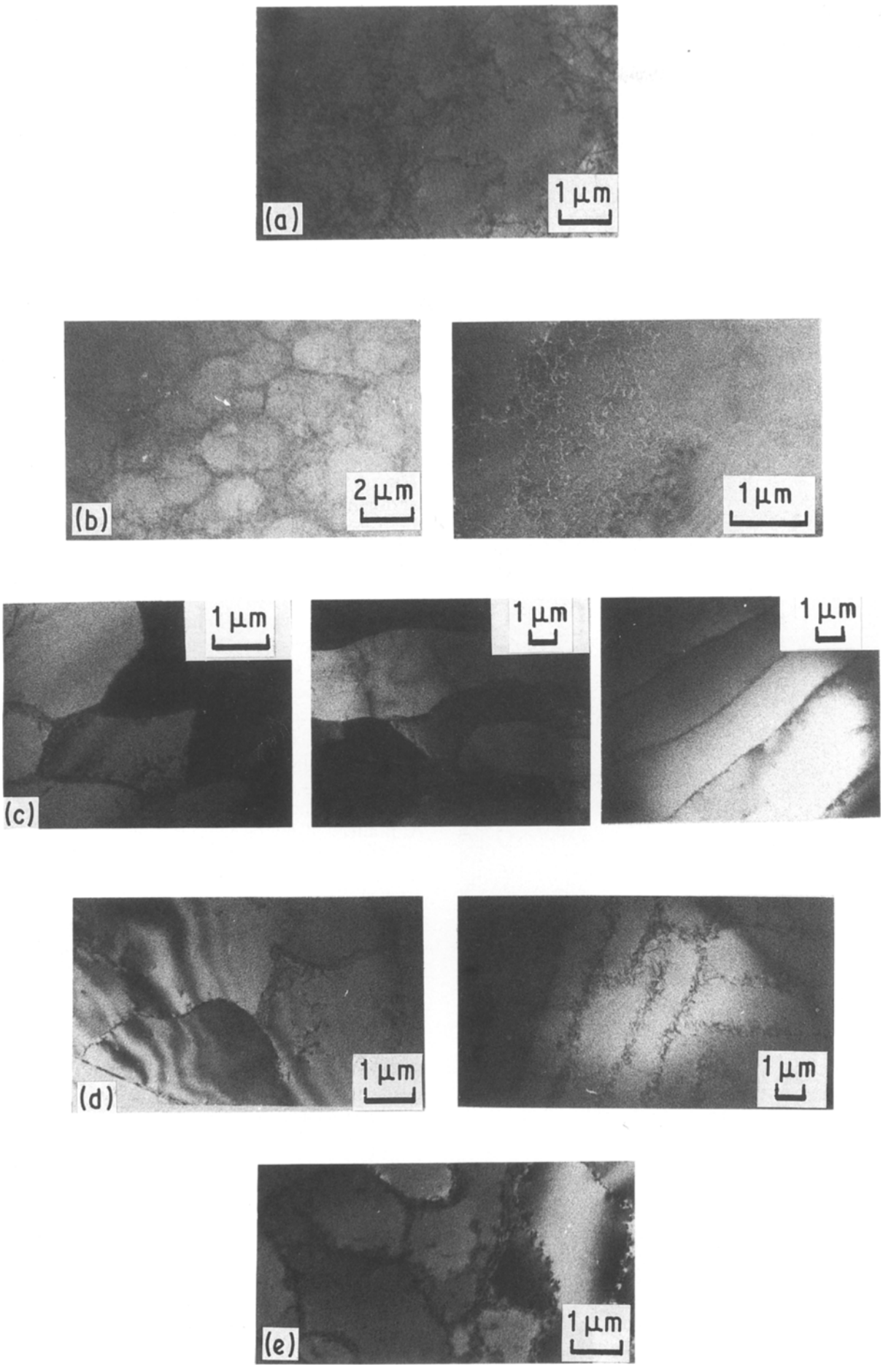

Figure 7 Al–0.7% alloy (TEM observation). (a) $\Delta\varepsilon_p/2 = 5 \times 10^{-5}$; loose cell structure ($\boldsymbol{g} = \langle 2\,0\,0 \rangle$). (b) $\Delta\varepsilon_p/2 = 3 \times 10^{-4}$; sharper cell structure (right cell wall in weak beam conditions ($\boldsymbol{g} = \langle 1\,1\,1 \rangle$). (c) $\Delta\varepsilon_p/2 = 8 \times 10^{-4}$; $\boldsymbol{g} = \langle 1\,1\,1 \rangle$: left, equiaxial cells ($\boldsymbol{g} = \langle 1\,1\,1 \rangle$); middle, elongated cells ($\boldsymbol{g} = \langle 1\,1\,1 \rangle$); right, channel structure. (d) $\Delta\varepsilon_p/2 = 10^{-3}$; $\boldsymbol{g} = \langle 2\,0\,0 \rangle$: left, equiaxial cells; right, labyrinth structure. (e) $\Delta\varepsilon_p/2 = 7.5 \times 10^{-3}$; $\boldsymbol{g} = \langle 2\,0\,0 \rangle$, cell structure.

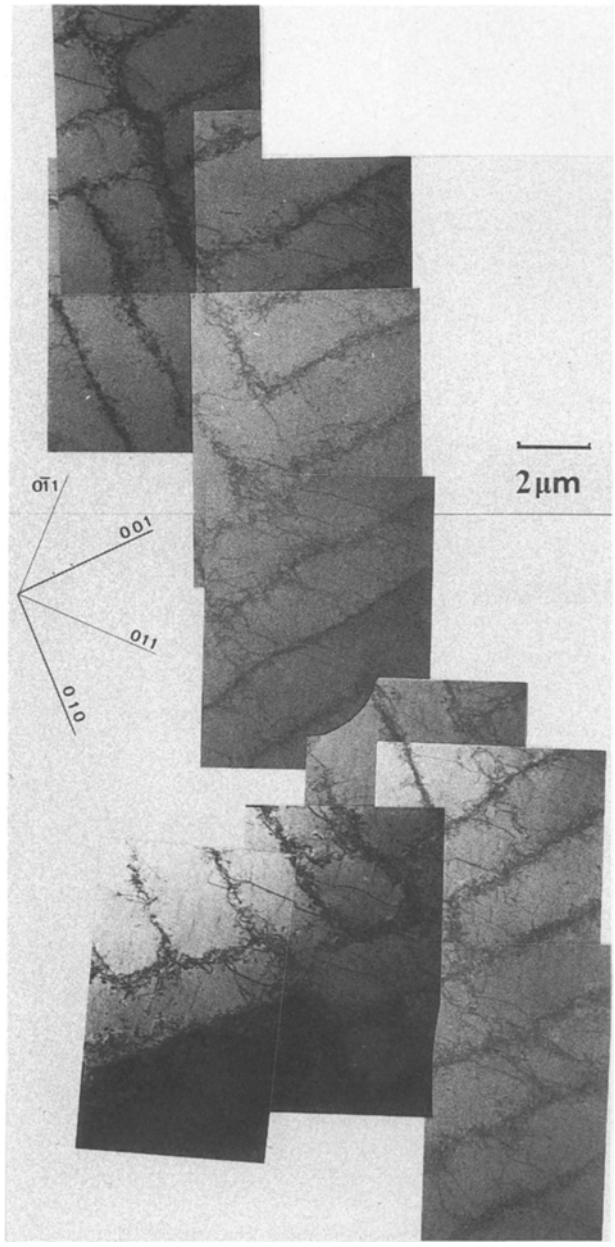

Figure 8 Al–0.7% alloy, $\Delta\varepsilon_p/2 = 10^{-3}$, foil plane {1 0 0}, $g = \langle 0\,2\,2\rangle$. Labyrinth structure, made of dislocation walls roughly perpendicular to $\langle 0\,0\,1\rangle$ directions. Long screw dislocations are observed in the channels.

again almost homogeneous and so is the dislocation structure. The only structure observed in that case is the cell structure with well-defined walls, but still the average cell size is about 1 to 2 μm (Fig. 7e).

The two structures found in the Al–0.7% Li alloy (cell structure and labyrinth structure) have been studied in their best defined form. The labyrinth structure (Fig. 7d) has its walls in crystallographic directions (Fig. 8) just as in polycrystalline copper. The cell structure, in the case of $1/2\Delta\varepsilon_p = 7.5 \times 10^{-3}$ in which walls are well defined, has been studied by the weak beam technique, showing three families of dislocation arranged in a wall in a sub-boundary structure (Fig. 9).

For the alloy with small shearable precipitates, deformation is always localized as shown previously by SEM but with two types of band. The two types of band correspond to two substructures.

In these alloys, whatever the amplitude of deformation, some bands free of δ' precipitates are always observed in the dark-field (Fig. 10). These bands and the way in which precipitates disappear have been extensively studied elsewhere [6]: it has been shown that they were deprived of δ' precipitates and impoverished in lithium. They lie parallel to {1 1 1} glide planes and correspond to easy glide for dislocations. Their width and spacing can be correlated to the width and spacing of slip lines and seem to be almost invariant when $\Delta\varepsilon_p$ changes.

The second type of localization (bands) is also associated with a typical substructure. Precipitate-free bands are still present but they are sometimes in groups (Fig. 11), the width and the spacing of which is now correlated with the width and the spacing of deformation bands observed on the surface by SEM.

4. Discussion: strain localization

A systematic study of surface aspect and microstructure (dislocations and precipitates) allows a correlation between microstructures and localization: when deformation is inhomogeneous, the microstructure is itself inhomogeneous at the microscopic scale. In the particular case of fatigue of Al–Li alloys, two factors are involved in localization of plastic deformation. On the one hand, fatigue testing is well known to lead to strain localization even in homogeneous materials as copper or aluminium [7], but on the other hand, the presence of a shearable precipitation, δ', also has a localizing effect even in monotonic straining. This second effect comes from the fact that when a precipitate is cut, its average radius in the slip plane is reduced, and therefore it can easily be cut again. More precisely, every shearing event of a δ' precipitate either creates an antiphase boundary (APB), or erases an APB already lying on the slip plane.

Statistically, an increasing number of APBs are created as the cumulative strain increases, and so does the number of steps at the precipitate/matrix interface. It can be easily understood that the resulting additional energy can displace the equilibrium radius of the precipitate, leading to dissolution [5]. This process is balanced by coarsening, which is itself helped by the high vacancy concentration resulting from fatigue straining. On this basis, it can be shown [5] that this type of strain localization by precipitate shearing is not governed by the strain amplitude, but by the strain rate. The related localization (slip lines) is therefore independent of $\Delta\varepsilon_p$. On the contrary, localization by fatigue is governed (at least in face centred cubic metals) by the strain amplitude. The strain domain in which we observe slip bands in Al–2.5% Li alloy ($1/2\Delta\varepsilon_p \simeq 10^{-3}$) is about the same as the domain in which we observe strain localization in Al–0.7% Li alloys ($1/2\Delta\varepsilon_p \simeq 10^{-3}$): "slip bands" are probably an effect of fatigue straining and slip lines an effect of strain localization by shearing. The loss of mechanical resistance observed for the underaged 2.5% Li alloy is probably due to the sharp strain localization resulting from precipitate shearing.

5. Conclusion

Two types of slip band, corresponding to two types of

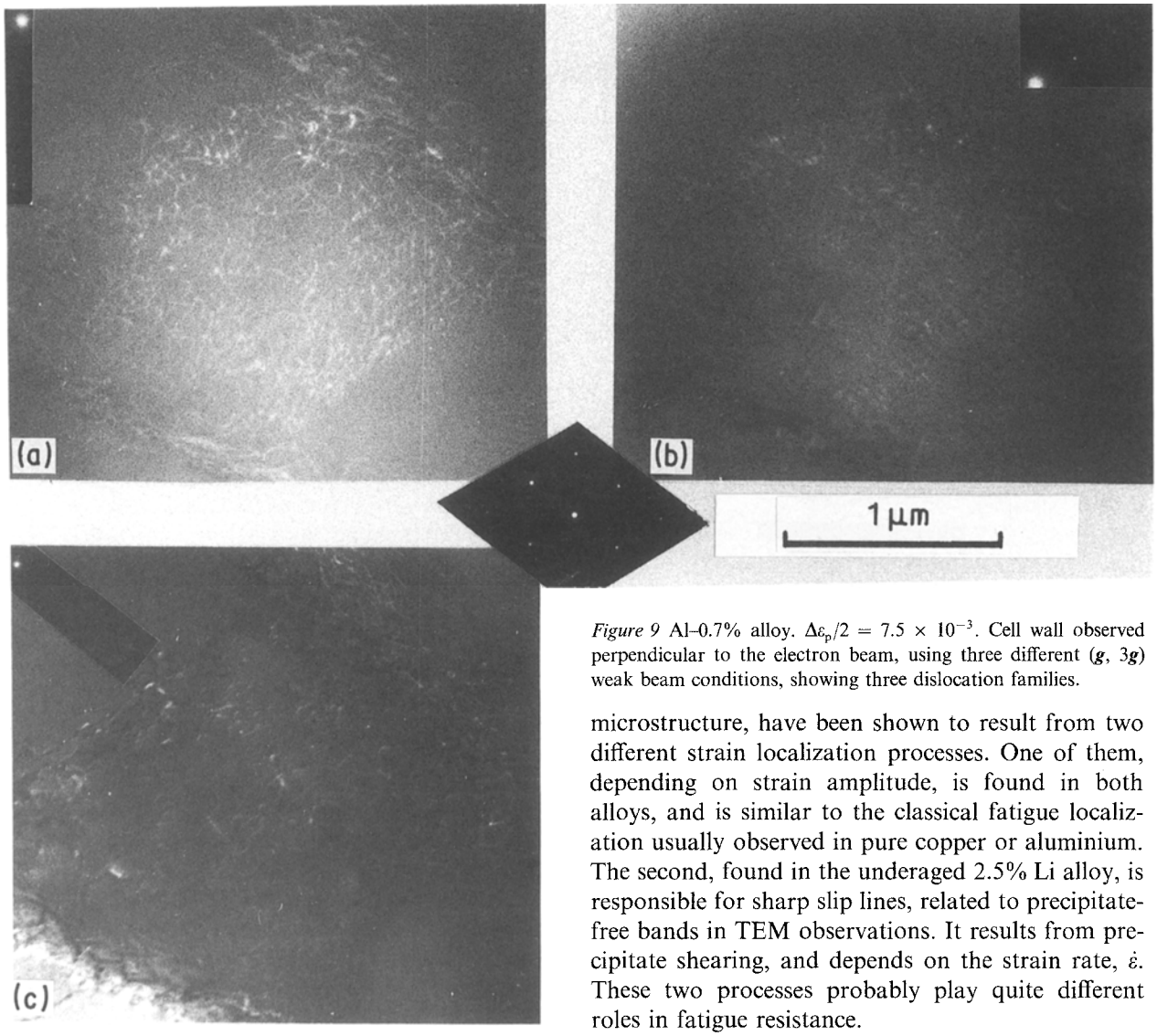

Figure 9 Al–0.7% alloy. $\Delta\varepsilon_p/2 = 7.5 \times 10^{-3}$. Cell wall observed perpendicular to the electron beam, using three different ($\boldsymbol{g}$, $3\boldsymbol{g}$) weak beam conditions, showing three dislocation families.

microstructure, have been shown to result from two different strain localization processes. One of them, depending on strain amplitude, is found in both alloys, and is similar to the classical fatigue localization usually observed in pure copper or aluminium. The second, found in the underaged 2.5% Li alloy, is responsible for sharp slip lines, related to precipitate-free bands in TEM observations. It results from precipitate shearing, and depends on the strain rate, $\dot{\varepsilon}$. These two processes probably play quite different roles in fatigue resistance.

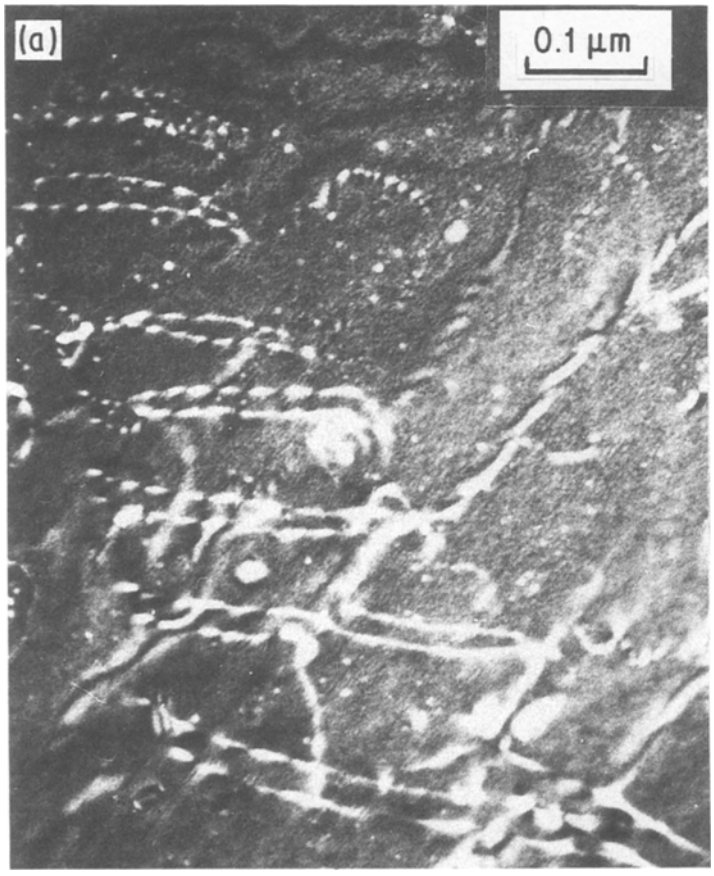

Figure 10 Al–2.5% alloy, aged at room temperature. $\Delta\varepsilon_p/2 = 8 \times 10^{-4}$. (a) Superdislocations, observed in ($\boldsymbol{g}$, $-\boldsymbol{g}$) weak beam conditions. (b) $\langle 1\,0\,0 \rangle$ superlattice dark-field (zone axis $\langle 0\,1\,1 \rangle$), showing precipitate-free bands (black stripes). Superdislocations are seldom observed when precipitate-free bands are well developed.

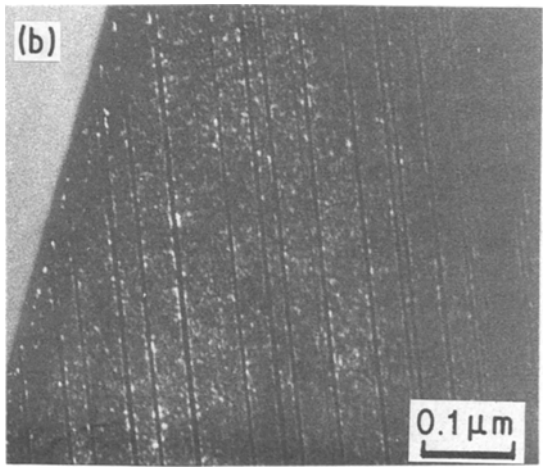

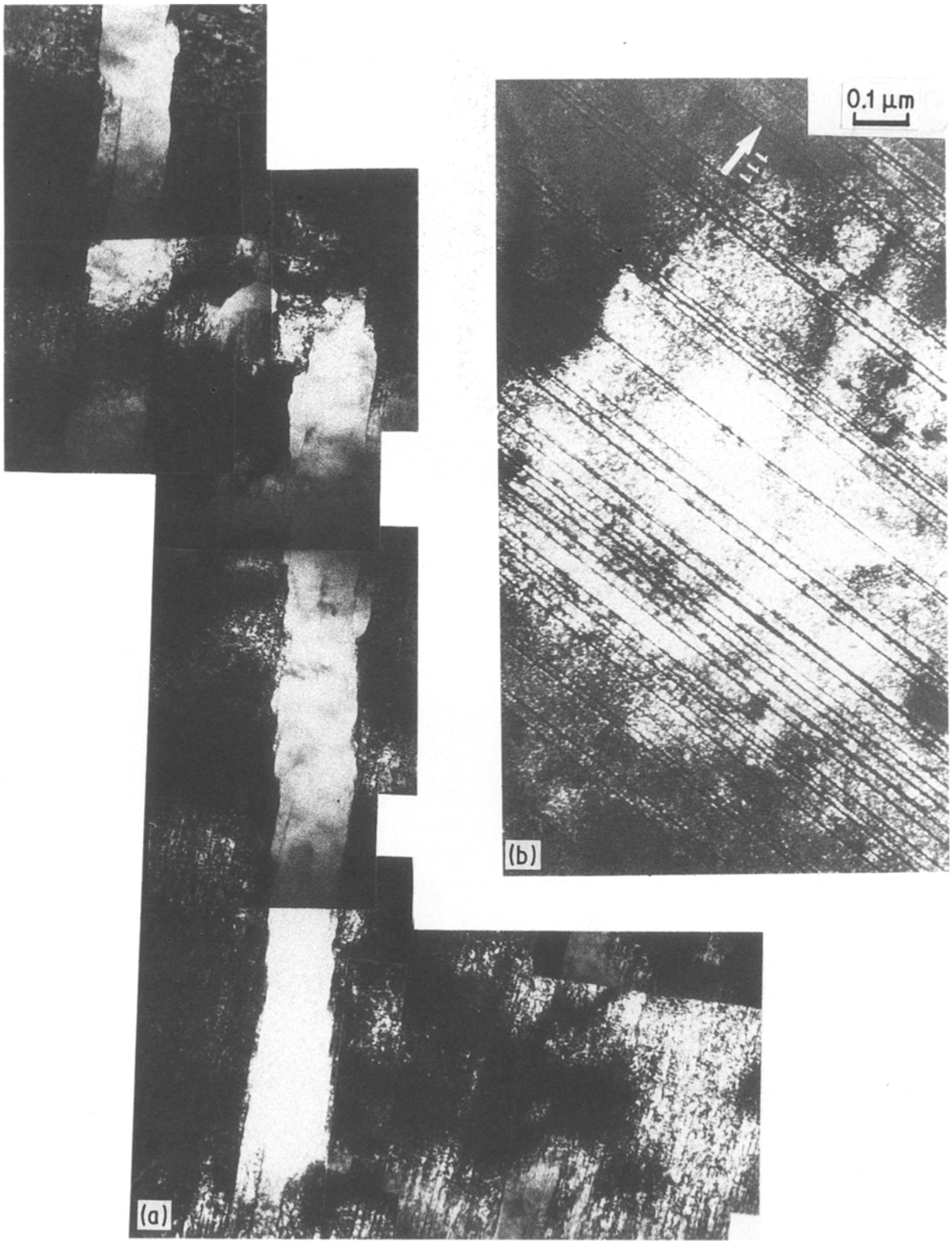

Figure 11 Al–2.5% alloy, aged 8 h at 100° C, and fatigued in torsion with a total strain amplitude $\Delta\varepsilon_t/2 = 3 \times 10^{-3}$. (a) $\boldsymbol{g} = \langle 2\,2\,0 \rangle$: deformation is planar, and slip bands are grouped in bundles. (b) Superlattice dark-field ($\boldsymbol{g} = \langle 1\,1\,0 \rangle$) showing precipitate-free bands.

Acknowledgements

The authors thank Pechiney for provision of the materials and for financial support of one of us (Y. B.).

References

1. C. CALABRESE, C. LAIRD, *J. Mater. Sci. Engng.* **13** (1974) 141.
2. R. STOLTZ and A. PINEAU, *ibid.* **34** (1978) 275.
3. J. DHERS, Thesis, St Etienne University (1986).
4. A. HUNSCHE and P. NEUMANN, *Acta Metall.* **34** (1986) 207.
5. J. LEPINOUX, Thèse d'Etat, Poitiers (1987).
6. Y. BRECHET, F. LOUCHET, C. MARCHIONNI and J. L. VERGER-GAUGRY, *Phil. Mag. A* **56** (1987) 353.
7. A. T. WINTER, *ibid.* **30** (1974) 719.

Received 24 May
and accepted 12 September 1988